



A EUROPEAN JOURNAL OF CHEMICAL BIOLOGY

CHEM **BIO** CHEM

SYNTHETIC BIOLOGY & BIO-NANOTECHNOLOGY

Accepted Article

Title: Ruthenium(II)-Arene Thiocarboxylates: Identification of a Stable Dimer Selectively Cytotoxic to Invasive Breast Cancer Cells

Authors: Liam Stephens, Aviva Levina, Iman Trinh, Victoria Blair, Melissa Werrett, Peter Lay, and Philip Andrews

This manuscript has been accepted after peer review and appears as an Accepted Article online prior to editing, proofing, and formal publication of the final Version of Record (VoR). This work is currently citable by using the Digital Object Identifier (DOI) given below. The VoR will be published online in Early View as soon as possible and may be different to this Accepted Article as a result of editing. Readers should obtain the VoR from the journal website shown below when it is published to ensure accuracy of information. The authors are responsible for the content of this Accepted Article.

To be cited as: *ChemBioChem* 10.1002/cbic.201900676

Link to VoR: <http://dx.doi.org/10.1002/cbic.201900676>

WILEY-VCH

www.chembiochem.org

A Journal of



Ruthenium(II)-Arene Thiocarboxylates: Identification of a Stable Dimer Selectively Cytotoxic to Invasive Breast Cancer Cells

Liam J. Stephens,^[a] Aviva Levina,^[b] Iman Trinh,^[a] Victoria L. Blair,^[a] Melissa V. Werrett,^[a]

Peter A. Lay,^{*[b]} and Philip C. Andrews,^{*[a]}

Abstract: Ru(II)-arene complexes provide a versatile scaffold for novel anti-cancer drugs. A new series of Ru(II)-arene-thiocarboxylato dimers **1-7** were synthesized and characterized. Three of the complexes (**2a**, **b** and **5**) showed promising anti-proliferative activities in MDA-MB-231 (human invasive breast cancer) cells, and were further tested in a panel of fifteen cancerous and non-cancerous cell lines. Complex **5** showed moderate but remarkably selective activity in MDA-MB-231 cells ($IC_{50} = 39 \pm 4 \mu\text{M Ru}$). Real-time proliferation studies showed that **5** induced apoptosis in MDA-MB-231 cells but had no effect in A549 (human lung cancer, epithelial) cells. By contrast, **2a** and **b** showed moderate anti-proliferative activity, but no apoptosis, in either cell line. Selective cytotoxicity of **5** in aggressive, mesenchymal-like MDA-MB-231 cells over many common epithelial cancer cell lines (including non-invasive breast cancer MCF-7) makes it an attractive lead compound for the development of specifically anti-metastatic Ru complexes with low systemic toxicity.

Introduction

Despite significant advances in cancer treatment, metastasis remains the main obstacle for successful therapy and the main cause of cancer-related mortality.^[1, 2] Metastasis is caused by a subpopulation of cancer cells that are not only able to invade surrounding tissues, but are often resistant to conventional chemotherapy.^[1, 2] Specific targeting of aggressive cancer cells remains challenging, as shown by a recent screening of 301 known anti-cancer drugs against a panel of sixteen breast cancer cell lines.^[3]

As part of a global effort towards the design and development of specifically anti-metastatic drugs,^[2] certain Ru complexes, such as NAMI-A and RAPTA-T (Figure 1, Ru(III) coordination and Ru(II) organometallic complexes, respectively), have attracted attention.^[4, 5] Like well-established Pt(II) anti-cancer drugs (cisplatin, carboplatin and oxaliplatin),^[6] these complexes contain relatively labile chlorido ligands that can be exchanged for donor groups of proteins and nucleic acids.^[7-9] The greater affinity for

Ru-chlorido ligand substitution in biological media compared to those of Pt(II) complexes leads to predominant binding of Ru(II) or Ru(III) anti-metastatic drugs to biomolecules in the extracellular space, or at the cell surface, rather than to intracellular targets.^[8, 10-13] The resultant disruption in communication between the cell surface and extracellular matrix is thought to be the main cause of anti-metastatic activities of NAMI-A, RAPTA-T and related Ru complexes.^[8, 10-13] However, the high reactivity of NAMI-A in biological media has also led to Ru binding to non-target tissues, which has caused excessive side effects that led to withdrawal of the drug from Phase II clinical trials.^[11] The only Ru complex remaining in active clinical trials, IT-139 (Figure 1, also known as NKP-1339)^[14] is thought to have predominantly cytotoxic activity.^[13, 15, 16] However, the mode of action differs from that of conventional cytotoxicity of Pt anti-cancer drugs that are used in the clinic as there is little difference in activity between the Pt resistant phenotype and the non-resistant phenotype of related cell lines.^[17] This experience emphasizes the need for new metal complexes as drugs with anti-metastatic activities.^[11, 13]

Ruthenium(II) arene complexes of "piano-stool" geometry (including RAPTA-T, Figure 1)^[18] are among the most extensively studied metal-based anti-cancer drugs, due to their straightforward synthesis from commercially available precursors and a great variety of available ligands.^[19-21] Although such complexes predominantly contain *N*, *O*, or *P*-donor ligands,^[19] a notable series of thiolato-bridged Ru(II) arene dimers has been developed by Furrer, Süss-Fink and co-workers.^[20, 21] In particular, trithiolato dimers, such as those shown in Figure 1, are stable under biological conditions, and are highly cytotoxic (IC_{50} values in nanomolar range) in common cancer cell lines.^[22-25] The absence of easily hydrolysable ligands in these dimers (Figure 1) means that they are likely to act by a different mechanism to those of classical Pt(II) drugs,^[6] or the Ru drugs that have entered clinical trials, which also undergo rapid ligand exchange reactions.^[8, 26] A proposed mechanism is based on their efficient cellular uptake (probably by passive diffusion through cell membranes due to the hydrophobic nature of the complexes),^[8, 9] followed by catalytic oxidation of cellular thiols by oxygen, leading to production of reactive oxygen species that cause cell death.^[21, 23, 27-29] Generally, these complexes were not selective for a particular cell type,^[22-24] although in one instance lower toxicity in lung cancer cells compared with breast cancer, or leukaemia cells was observed.^[25] The reasons for such selectivity were not further explored.

[a] Dr. L. J. Stephens, Dr. I. Trinh, Dr V. L. Blair, Dr. M. V. Werrett, Prof. P. C. Andrews
School of Chemistry, Monash University
Clayton, Melbourne, Vic, 3800 (Australia)
E-mail: phil.andrews@monash.edu

[b] Dr. A. Levina, Prof. P. A. Lay
School of Chemistry, University of Sydney
Eastern Avenue, Sydney, NSW 2006 (Australia)
E-mail: peter.lay@sydney.edu

Supporting information for this article is given via a link at the end of the document.

FULL PAPER

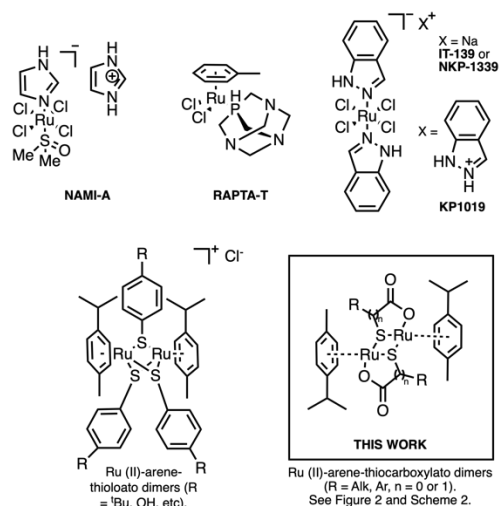


Figure 1. Typical structures of Ru complexes tested as anti-cancer drugs.^[4, 5, 15, 18, 21, 24, 25, 30]

In this work, we present the synthesis, purification, and comprehensive characterisation of a novel series of hydrolytically stable Ru(II)-arene-thiocarboxylato complexes, $[\text{Ru}(\text{p-cymene})\text{O}_2\text{C-CH}(\text{S})\text{-R}]_2$ (**1-3**) and $[\text{Ru}(\text{p-cymene})\text{O}_2\text{C-CH}_2\text{-CH}(\text{S})\text{-R}]_2$ (**4-7**) (Figure 1 and 2), derived from bifunctional α - and β -mercaptocarboxylic acids; thiosalicylic acid (**TLA-H₂**), (R)-2-mercapto-3-phenylpropanoic acid (**(R)-MPA-H₂**), (S)-2-mercapto-3-phenylpropanoic acid (**(S)-MPA-H₂**), (R)-2-mercapto-3-methylbutanoic acid (**(R)-MMA-H₂**), (S)-2-mercapto-3-methylbutanoic acid (**(S)-MMA-H₂**), 3-mercapto-3-phenylpropanoic acid (**MBA-H₂**), 3-mercapto-3-phenylpropanoic acid (**MPP-H₂**), 3-mercapto-3-(4-methoxyphenyl)propanoic acid (**MMPA-H₂**) and thiosalicylic acid (**TSA-H₂**) (Figure 2). The anti-proliferative activities of all the complexes (**1-7**) were studied in various types of cultured mammalian cells.

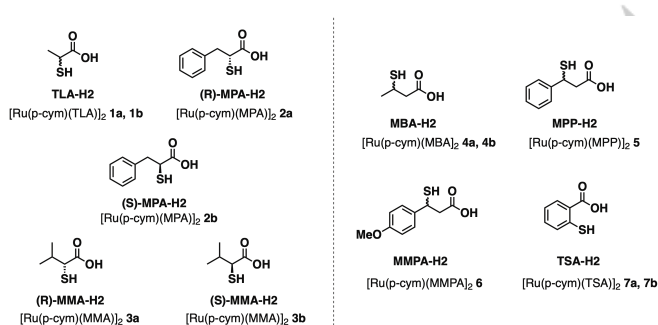


Figure 2. The five α -mercaptocarboxylic acids (left) and four β -mercaptocarboxylic acids (right) used for complexation with $[\text{RuCl}_2(\text{p-cymene})]_2$ and their corresponding complex formula and code.

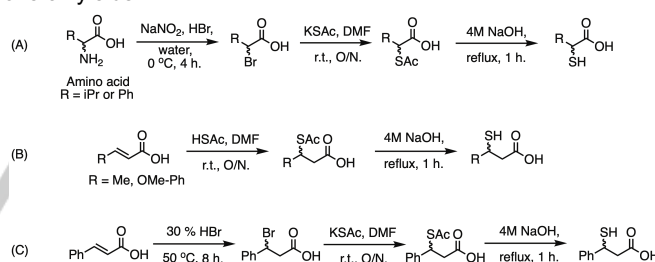
Although these complexes mostly showed low to moderate activities in the studied cell lines, remarkably one of them (**5**) was selectively cytotoxic to a highly invasive human breast cancer cell

line (MDA-MB-231),^[31] while having little or no effect in most non-invasive cancer or non-cancer cell lines. These results show considerable promise in the challenging area of treating aggressive types of breast cancer.^[2, 3]

Results and Discussion

Synthesis of α and β -mercaptocarboxylic acids. α -Mercaptocarboxylic acids were derived from the D- and L-isomeric forms of valine and phenylalanine respectively, via a three-step reaction process (Scheme 1-A).^[32] The first step in this sequence involved the substitution of the amino acid amine functionality with bromine using HBr and NaNO_2 . Once in hand, the α -bromo carboxylic acids were exposed to a nucleophilic attack from potassium thioacetate, before subsequent deprotection of this moiety resulted in the formation of the desired α -mercaptocarboxylic acids in good overall yields.

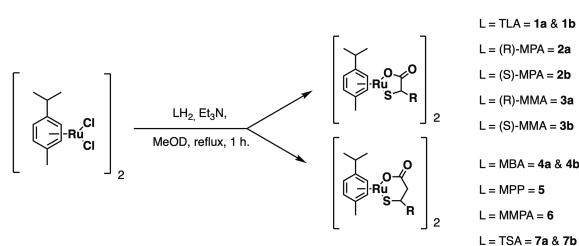
The β -mercaptocarboxylic acids were derived from α,β -unsaturated carboxylic acids via a two- (Scheme 1-B) or three-step reaction process (Scheme 1-C).^[33] The first step in this sequence involved the Michael addition of either potassium thioacetate or HBr to the α,β -unsaturated acid. The intermediate bromo compound formed from cinnamic acid then underwent nucleophilic attack using potassium thioacetate resulting in the formation of the thioacetate functionality in excellent yield. The 3-(acetylthio)carboxylic acids were then deprotected under basic conditions, to give the desired β -mercaptocarboxylic acids in good overall yields.



Scheme 1. General synthesis of α -(**A**) and β -mercaptocarboxylic acids (**B** and **C**).

Synthesis of ruthenium complexes. A previous study by Henderson *et al.* demonstrated that the dimeric complex, $[\text{Ru}(\text{p-cymene})(\text{TSA})_2]_2$, could be formed from the treatment of $[\text{RuCl}_2(\text{p-cymene})]_2$ with thiosalicylic acid (TSA).^[34] This method, which involved treatment of $[\text{RuCl}_2(\text{p-cymene})]_2$ with the acid in methanol and excess Et_3N , under reflux for one hour, was initially applied in the synthesis of our target $[\text{Ru}(\text{p-cymene})\text{L}]_2$ complexes, using the broader range of mercaptocarboxylic acids (Scheme 2).

FULL PAPER



Scheme 2. General synthesis of ruthenium (II) (*p*-cymene) thiocarboxylato complexes **1-7**.

However, attempts to isolate complexes of high purity and in high yield proved problematic; ^1H NMR spectra indicated a number of presently unidentified species in the crude solution. The crude mixtures were therefore purified using silica gel chromatography. For each of the crude products, two separate light-orange bands were eluted off the column ($R_f \sim 0.90$ and 0.26) and a dark brown band was retained on the column at $R_f = 0$ (Figure S1). Mass spectrometry on each of the two light-orange bands collected, showed them to have the same molecular mass, composition, and fragmentation pattern, and to exist as dimers in the solution state, $[\text{Ru}(p\text{-cymene})\text{L}]_2$. However, ^1H and ^{13}C NMR spectra on the two bands showed significant chemical shift differences (see Figure 3 as a representative example); both of which were consistent with previously reported Ru(II) *p*-cymene complexes, in that the aromatic *p*-cymene signals appeared as four independent doublets, whilst the *iso*-propyl methyl signals appeared as two inequivalent doublets arising from the unsymmetrical Ru centre (see Supporting Information for NMR spectra for all complexes).

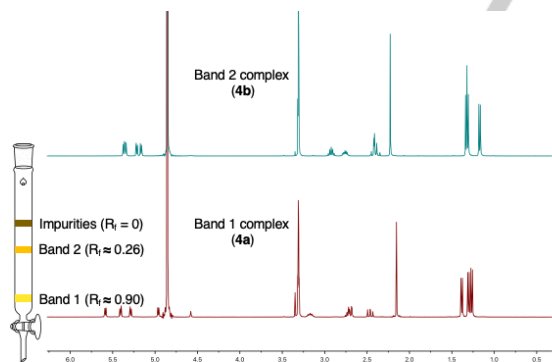


Figure 3. ^1H NMR spectra for complex **4a** (bottom) and complex **4b** (top), both synthesized from the β -mercaptocarboxylic acid; **MBA-H₂**.

Despite the use of prep-HPLC as an additional purification step, ^1H NMR spectroscopy on the two bands obtained on the complexes derived from **MPA-H**, **MMA-H**, **MPP-H** and **MMPA-H**, showed only one to be an analytically pure complex with the 'second band' composed of traces of a number of presently unidentified species. Hence, the 'second band' of these complexes were discarded for use in biological studies.

Structure elucidation. Single crystal X-ray diffraction revealed that complexes **1a**, **2b**, **3b**, **4a**, **5**, **6** and **7a** (obtained from the first eluted band) are dimeric in the solid-state and adopt a pseudo octahedral 'piano-stool' geometry consisting of central Ru_2S_2 units formed by two bridging thiolates.^[34] Unfortunately, the structures of complexes **1b**, **4b** and **7b**, complexes obtained from the second eluted band, have not been amenable to producing crystals suitable for X-ray crystallography, as yet. The use of both 2D NMR and Raman spectroscopy did not elicit any additional information with regards to their particular structure and chemical composition.^[35] First reported by Deacon *et al.*, IR spectroscopy and in particular the carbon-oxygen stretching frequencies can be used to diagnose the nature of carboxylate coordination to a metal centre.^[36] Resulting from the inequivalence of the two oxygen atoms, it has been demonstrated that unidentate coordination of the carboxylate ligand results in an increase in $\nu_{\text{asym}}(\text{CO}_2)$, a decrease in $\nu_{\text{sym}}(\text{CO}_2)$ and hence the separation (Δ) between the two C-O stretching frequencies is larger in comparison to the free carboxylate ion.^[36] Deacon *et al.* report that Δ values of separation for unidentate coordination are typically larger than 200 cm^{-1} , whilst bidentate coordination typically give much lower values. The spectra obtained for complexes **4a** and **4b** suggest a different carboxylate coordination to the Ru centre, with the Δ value of separation for complex **4a** observed as 215 cm^{-1} (unidentate) whilst the equivalent value for complex **4b** was observed as 151 cm^{-1} (bidentate). As a result of this finding, we hypothesise that complexes **1b**, **4b** and **7b** exist as dimers in which each *p*-cymene Ru centre is bound to an $\text{O}_2\text{O}'$ chelate and a thiolate (Figure 4). To further probe this hypothesis, multiple scattering analysis of XAS data may be able to differentiate between different possible structures. This will be the subject of future works.^[37]

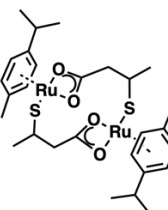


Figure 4. Proposed structure of complex **4b**.

X-Ray crystallography. Of the twelve Ru(II)-arene thiocarboxylato complexes synthesized, **1a**, **2b**, **3b**, **4a**, **5**, and **6** were amenable to single crystal diffraction studies on crystals grown from methanol/ethanol layered water or DMSO solutions. The crystal structure of complex **7a** has been described previously.^[34] Pertinent bond lengths and distances are outlined in Table 1 and a full summary of the crystallographic data is provided in the Experimental section. All six Ru-thiocarboxylato complexes are isostructural with the ligand being dianionic having doubly deprotonated at the thiol and hydroxy functionalities to give chelated dimeric complexes; $[\text{Ru}(p\text{-cymene})(\text{TLA})]_2$ **1a**, $[\text{Ru}(p\text{-cymene})(\text{MPA})]_2$ **2b**, $[\text{Ru}(p\text{-cymene})(\text{MMA})]_2$ **3b**, $[\text{Ru}(p\text{-cymene})(\text{MBA})]_2$ **4a**, $[\text{Ru}(p\text{-cymene})(\text{MPP})]_2$ **5** and $[\text{Ru}(p\text{-cymene})(\text{MMPA})]_2$ **6**. The solid-state structures of complexes **1a**

FULL PAPER

and **5** are shown in Figures 5 and 6, whilst complexes **2b**, **3b**, **4a** and **6** are shown in the Supporting Information (Figures S2-S5).

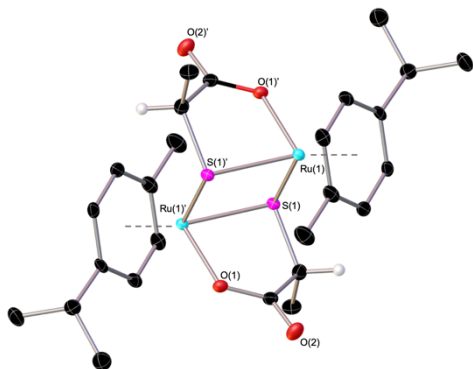


Figure 5. Molecular structure of $[\text{Ru}(\textit{p}\text{-cymene})(\text{TLA})]_2 \cdot 2\text{H}_2\text{O}$ **1a**. Hydrogen atoms (except C-H backbone ones) and uncoordinated solvent molecules omitted for clarity. Thermal ellipsoids show at 40 % probability. Symmetry operator: $-x, 1-y, 1-z$.

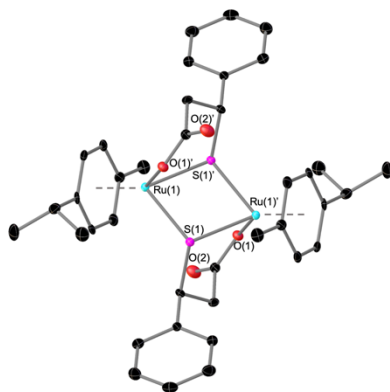


Figure 6. Molecular structure of $[\text{Ru}(\textit{p}\text{-cymene})(\text{MPP})]_2$ **5**. Hydrogen atoms and uncoordinated solvent molecules omitted for clarity. Thermal ellipsoids show at 40 % probability. Symmetry operator: $-x, -y, -z$.

Complexes **1-3** and **4-6** can be viewed as $[\text{Ru}(\textit{p}\text{-cymene})(\text{L})]$ ($\text{L} = \text{TLA}, \text{MBA}, \text{MPA}, \text{MBA}, \text{MPP}$ or MMPA respectively) monomers connected by bridging Ru-S bonds (average bond length = 2.3859 Å), with the Ru metal atom O,S-chelated to form a RuSOC_2 five-membered ring in the α -thiocarboxylato complexes **1-3** or a six-membered RuOSC_3 ring in β -thiocarboxylato **4-6**. Dimerisation through Ru-S bonds leads to a planar central Ru_2S_2 core, while the coordination sphere of the Ru(II) atom is completed by an η^6 -*p*-cymene coordinated molecule giving an overall distorted tetrahedral geometry. The bond parameters and geometries in **1-3** and **4-6** are comparable with the previously reported thiocarboxylato Ru complex $[\text{Ru}(\textit{p}\text{-cymene})(\text{TSA})]_2$, **7a** (Table 1).^[34]

Table 1. Selected comparative bond lengths (Å) and angles (°) of complexes **1-7**.

	1a	2b	3b	4a	5	6	7a
Ru-S	2.375 3(9)	2.375 3(11)	2.379 4(14)	2.381 8(16)	2.394 0(8)	2.376 8(4)	2.384 8(4)
Ru-S'	2.391 4(10)	2.391 3(12)	2.377 4(14)	2.384 6(16)	2.388 6(8)	2.385 3(4)	2.417 7(4)
Ru-O	2.109(2)	2.094(3)	2.099(4)	2.111(4)	2.111(4)	2.104(10)	2.093(12)
Ru-C _{cen} troid	1.969	1.687	1.679	2.186	2.210(3)	1.691	
S-Ru-S'	81.35(4)	80.67(4)	81.34(5)	81.41(6)	80.95(3)	79.79(13)	80.71(15)
S-Ru-O'	80.88(7)	80.67(8)	81.43(10)	86.87(14)	87.15(6)	87.27(3)	87.80(4)
S'-Ru-O	80.42(7)	80.31(8)	81.25(9)	77.77(14)	76.53(6)	76.14(3)	77.80(4)

Stability and anti-proliferative activity of complexes **1-7**.

Activity of complexes **1-7** against MDA-MB-231 and A549 cell lines.

Preliminary studies compared the effects of **1-7** (10–100 μM Ru, 72–96 h) on the proliferation rates of two contrasting human cancer cell lines: (i) MDA-MB-231 (breast cancer, mesenchymal-like, highly invasive)^[3, 31] and (ii) A549 (lung cancer, epithelial, non-invasive in the absence of growth factor stimulation),^[38] using real-time observations with IncuCyte Zoom imaging system.^[39, 40] Typical results (Figures S6 and S7, Supporting Information) indicated that only **2a,b** and **5** (i.e., the complexes that contained phenyl groups in the ligands, Schemes 1 and 2) had promising anti-proliferative activities at ~ 50 μM Ru. All the complexes with aliphatic substituents in the ligands (**1a,b**, **3a,b** and **4a,b**) had little or no activity at ~ 100 μM Ru, while the use of **6** and **7a,b** was limited by their low solubility in organic solvents (DMF or DMSO) that were used to prepare stock solutions for cell assays.^[41] All the mercaptocarboxylic acids used as precursors to **1-7** (Figure 2) had no significant anti-proliferative effect on either MDA-MB-231 or A549 cells at 100 μM for 72 h (data not shown).

Complexes **1-7** retained dimeric structures under biomimetic conditions (50 μM Ru, 10 mM aqueous NH_4HCO_3 , pH 7.5, stored for up to a week at 295 K),^[40, 42] as shown by ESI-MS (Figure S8 in Supporting Information). These results contrast those for typical metal complexes that rapidly decompose under cell culture conditions.^[9, 40, 42, 43] Stock solutions of **1-7** used in the ESI-MS studies (2–20 mM Ru in DMF) were stored for about a month in the dark at 295 K prior to the dilution with 10 mM NH_4HCO_3 . This observation confirms that the DMF stock solutions of Ru(II) are thiocarboxylato dimers were also stable, which is an important consideration for cell culture assays.^[9, 44]

Activity of **2a,b and **5** in various cell types.** Based on the preliminary results (Figure S6), the anti-proliferative activities of **2a,b** and **5** were compared in a broader range of cell lines (Table

FULL PAPER

2). An endpoint colorimetric MTT assay (MTT = 3-(4,5-dimethylthiazol-2-yl)-2,5-diphenyltetrazolium bromide)^[45] was used instead of IncuCyte observations, because it allowed to test the non-adherent and semi-adherent cell lines, such as THP-1, HL-60 and HepG2 (Table 2). This or similar assays have been widely used previously to assess the anti-proliferative activity of metal complexes, including Ru-arene-thiolato dimers.^[22-25] All the cell lines were treated for 72 h with $50 \pm 5 \mu\text{M}$ Ru (verified by atomic absorption spectroscopy, see Experimental Section). A summary of results is presented in Figure 7. Compound **1b** that showed a weak but statistically significant activity in A549 cells in preliminary experiments (Figure S6) was also tested in all the cell lines listed in Table 2, but the resultant cell viabilities were $\geq 80\%$ of control and are not included into Figure 7.

Most strikingly, **5** showed the greatest proliferation inhibition in mesenchymal-like^[31] MDA-MB-231 cells (No. 3 in Figure 7) while having little effect in all the studied epithelial and fibroblastic cells, with the exception of A2780 (ovarian cancer, No. 6 in Figure 7). Concentration-dependent studies of **5** in MDA-MB-231 cells (Figure S7) have shown that the complex did not change its activity ($IC_{50} = 39 \pm 4 \mu\text{M}$ Ru) after 72 h pre-incubation with fully supplemented cell culture medium (Experimental Section) at 310 K and 5% CO₂. This result, in conjunction with ESI-MS data (Figure S8), confirms that **5** was stable for the duration of cell culture assays. Differences in action of **2a,b** in various cell types were less prominent (Figure 7), and no consistent differences were observed between the activities of these two complexes that were derived from enantiomeric ligands.

Generally, higher activities of **2a,b** and **5** were observed in blood-derived or mesenchymal-like^[31, 46, 47] cells compared with epithelial or fibroblastic cells (Nos. 1-5 vs. 6-15 in Figure 7 and Table 2). Such selectivity is remarkable since mesenchymal cells and fibroblasts share many morphological and biochemical characteristics.^[48] No major differences in activity were observed between cisplatin-resistant and sensitive A2780 cells (Nos. 5 and 6 in Figure 7 and Table 2).^[47, 49] Like previous results for Ru(II)-arene-trithiolato dimers,^[22] this suggests that **2a,b** and **5** act by a different mechanism compared to Pt(II) drugs.^[6, 9, 21] However, the mechanisms of action of these two types of Ru(II) dimers are unlikely to be the same, since typical trithiolato complexes were more toxic in MCF-7 (epithelial, non-invasive breast cancer cells)^[31] than in MDA-MB-231 cells,^[24, 25] while the opposite trend was observed for **2a,b** and **5** (Nos. 3 and 9 in Figure 7 and Table 2).

Among the epithelial cell lines studied (Nos. 6-13 in Figure 7 and Table 2), there were no consistent differences in the effects of **2a,b** and **5** in immortalized non-cancer (HEK-293 and BEAS-2B, Nos. 7 and 10) compared with cancer cells. Similarly, previous studies^[23] showed no differences in the effects of Ru(II)-arene-trithiolato dimers in A2780 and HEK-293 cells. However, **2a,b** and **5** showed low toxicity in normal rodent fibroblasts (V79-4 and 3T3-L1 cell lines, Nos. 14 and 15 in Figure 7 and Table 2), which points to possible selectivity for cancer versus rapidly growing non-cancer cells.^[26]

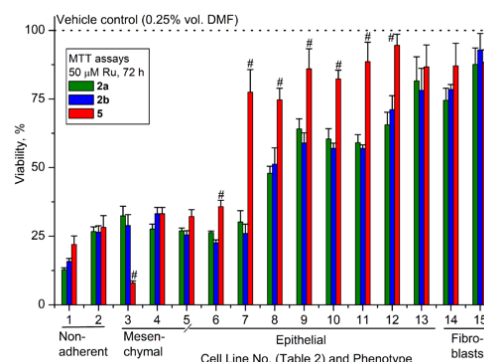


Figure 7. Comparison of anti-proliferative activities (MTT assays) of **2a,b** and **5** in a panel of cancer and non-cancer cell lines (Table 2). Stock solutions of Ru complexes in DMF (20 mM Ru, DMF) were diluted 400-fold with growth medium (Advanced DMEM with 2% vol. FCS) immediately before the 72 h treatments. Final Ru concentrations in the medium were $50 \pm 5 \mu\text{M}$ (GFAAS). Error bars represent mean values and standard deviations of two independent experiments, each including six replicate wells ($n = 12$). The # signs represent highly significant differences ($P < 0.001$) of the effect of **5** from the average effect of **2a** and **2b**.

Anti-proliferative vs. Cytotoxic activity of 2a,b and 5. Typical cell proliferation assays, including MTT assays, are based on measuring bulk cell metabolism,^[45] and do not differentiate between anti-proliferative and cytotoxic activities of anti-cancer drugs.^[3] Preliminary morphological observations using IncuCyte Zoom imaging system (Figure S9) indicated that **5** ($\sim 50 \mu\text{M}$ Ru) caused death of MDA-MB-231 cells after 24 h incubation, while **2a** and **2b** slowed their growth, but the remaining cells were alive after 72 h incubations. This difference was explored further using fluorescent dyes that were designed for IncuCyte assays: (i) green fluorescent (excitation/emission = 500/530 nm) Caspase 3/7 reagent that is specific for early stage apoptotic cells;^[50] and (ii) red fluorescent (excitation/emission = 610/630 nm) Cytotox Red reagent that stains late stage apoptotic and necrotic cells with damaged membranes.^[51] A well-known cytotoxic Ru(III) complex, KP1019 (Figure 1)^[13, 30, 52] was used as a positive control. Figure S10 shows typical morphologies of viable (unstained), apoptotic (green)^[53] and late apoptotic or necrotic (red)^[54] MDA-MB-231 (**a**) and A549 (**b**) cells after 24-h treatments with $50 \mu\text{M}$ Ru (**5** or KP1019, respectively). Figure 8 shows the results of quantitative processing of cell confluence (**a,b**) and fluorescence (**c-f**) data. Fluorescence results in Figure 8 are presented as a proportion of green or red fluorescent cell area relative to total cell area (determined from phase contrast images), but similar time profiles were obtained using integrated green or red fluorescence intensities (Figure S11, Supporting Information).^[39]

FULL PAPER

In agreement with results from MTT assays (Nos. 3 and 11, Figure 7), treatment with **5** (50 μ M Ru) completely stopped the growth of MDA-MB-231 cells after 24 h, but had no significant effect on the growth rate of A549 cells compared with the control (black and red lines in Figure 8a,b). By contrast, **2a** and **2b** caused partial growth inhibition in both cell lines (green and blue lines in Figure 8a,b). In agreement with published data,^[52] KP1019 (50 μ M, freshly added to cell culture medium) completely stopped the proliferation of both cell lines (purple lines in Figure 8a,b). Concomitantly with the halt in MDA-MB-231 cell growth caused by **5**, there was a significant increase in the proportion of apoptotic cells (red lines in Figure 8a,c), while the treatments with **2a** or **2b** did not cause a significant degree of apoptosis (green and blue lines in Figure 8c). Treatment of MDA-MB-231 cells with KP1019 caused rapid growth in the proportion of apoptotic cells in the first 4 h of incubation, followed by slower decrease due to cell death and detachment (purple line in Figure 8c). In A549 cells, only treatment with KP1019 led to significant apoptosis (Figure 8d). As expected, time-dependent cell death profiles in both cell lines were similar but slower to proceed compared to those due to apoptosis (Figure 8e,f). Slow decays in red fluorescence registered by IncuCyte (Figure 8e,f) were due to the detachment of dead cells. In summary, the data within Figure 8 confirmed the striking difference in the effects of structurally similar compounds, **2a,b** and **5** (Figure 1 and Scheme 1), in two well-established human cancer cell lines (Table 2). Namely, **5** (50 μ M Ru) completely stopped the proliferation and triggered apoptosis in MDA-MB-231 cells but had no significant effect in A549 cells under the same conditions, while **2a** and **2b** caused partial inhibition of cell growth, but not apoptosis, in either cell line. The Ru concentration used is clinically relevant, as 0.10-0.40 mM Ru were detected in the blood plasma of patients receiving KP1019 during clinical trials.^[55] Notably, most of the known anti-cancer drugs are unable to cause apoptosis in aggressive breast cancer cell lines, including MDA-MB-231, at clinically relevant concentrations.^[3]

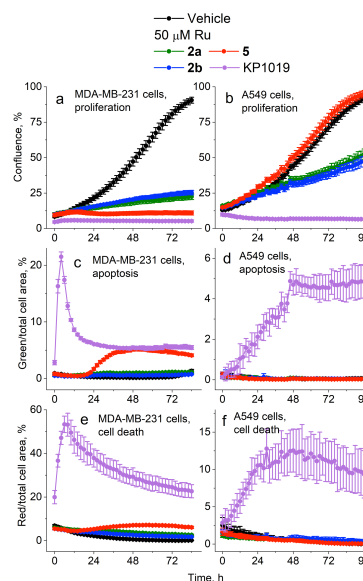


Figure 8. Typical time profiles of cell proliferation (a and b, phase contrast images), apoptosis (c and d, green fluorescence with Caspase 3/7 reagent)^[50] and cell death (e and f, red fluorescence with Cytotox reagent)^[51] in MDA-MB-231 or A549 cells in the presence or absence of 50 \pm 5 μ M Ru (**2a,b**, **5** or KP1019 as a positive control, IncuCyte Zoom imaging).^[52] Other cell culture conditions correspond to those in Figure 7. Error bars represent mean values and standard deviations of six replicate wells.

Uptake of Ru complexes by MDA-MB-231 and A549 cells.

Figure 9 compares the short-term (a, 50 μ M Ru for 4 h) and long-term (b, 20 μ M Ru for 72 h) uptake of **1b** (non-toxic in both cell lines), **2a,b** (anti-proliferative in both cell lines) and **5** (cytotoxic in MDA-MB-231, non-toxic in A549 cells). Treatment conditions were chosen based on the data contained within Figures 7, S5, 6 and 7, to avoid extensive cell death and detachment during the treatments. Both conditions led to significantly higher uptake of dimers that have phenyl residues in the ligands (**2a,b** and **5**) compared with **1b** that had methyl residue (Figure 1 and Figure 9). This feature is readily explained by the increased lipophilicity of aromatic ligands in **2a,b** and **5** and is likely to cause lower anti-proliferative activity of **1b** compared with the other complexes.^[8, 9, 52] The uptakes of **2a,b** or **5** by A549 cells were 5-30-fold lower than those by MDA-MB-231 cells under the same conditions (Figure 9), which is consistent with the lower toxicity of these compounds in the former cell line (Figures 7 and 8). Long-term uptake of lower Ru concentrations (Figure 9b) was 4-8-fold less efficient than short-term uptake of higher Ru concentrations (Figure 9a). This feature points to the existence of an active Ru efflux mechanism, probably through lysosomal uptake and exocytosis, which was previously described for Pt(II) complexes and other anti-cancer drugs.^[56] More intriguingly, the uptake of **2a** and **2b** by MDA-MB-231 cells was higher than that of **5**, although the difference was statistically significant only for the longer treatment time (Figure 9), which shows that the higher toxicity of

FULL PAPER

5 in this cell line compared with **2a,b** (Figures 7 and 8), has a specific mechanistic aspect that is unrelated to the level of Ru uptake in these complexes.

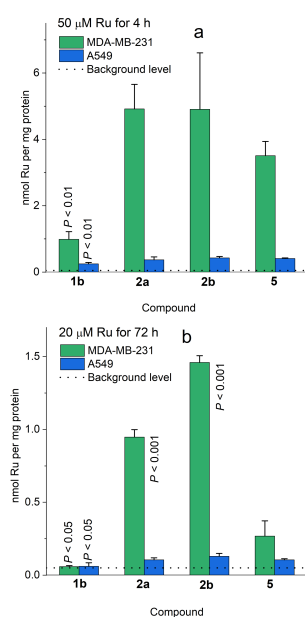


Figure 9. Ru uptake by MDA-MB-231 or A549 cells after short-term (a) or long-term (b) treatments with selected Ru arene thiocarboxylato complexes. Error bars represent means and standard deviations of three replicate samples. The *P* values indicate statistically significant differences in Ru uptake compared with compound **5** in the same cell line.

Implications for the use of **5 in cancer treatment.** The mesenchymal-like MDA-MB-231 (invasive breast cancer) cell line^[31] is a widely used in vitro model for the detection and treatment of metastatic cancers, particularly breast cancer.^[3, 57] High anti-proliferative activities in MDA-MB-231 cells ($IC_{50} < 1 \mu\text{M}$ Ru, 72 h treatment) have been reported for Ru(II)-arene-trithiolato dimers^[24, 25] and some monomeric Ru(II) and Os(II) arene complexes,^[58] which far surpassed the highest activity reported here for **5** (Figures 7 and 8). However, **5** is among a few reported metal complexes that were selective to MDA-MB-231 cells over common epithelial cancer cell lines,^[59] such as MCF-7 (non-invasive breast cancer),^[60] as well as over immortalized non-cancer epithelial cells,^[58] or normal fibroblasts^[61] (Table 2 and Figure 7). To our knowledge, there were no previous reports of metal complexes that showed selectivity for MDA-MB-231 cells over all three mentioned cell types. This selectivity is particularly remarkable, since it was not observed for two other Ru(II)-arene-thiocarboxylato dimers that are closely structurally related to **5** (**2a,b** in Figure 1 and Figure 7). Unlike for **2a** and **b**, **5** was able to trigger apoptosis in MDA-MB-231 (but not in A549) cells (Figure 8b,d). All three complexes are likely to retain their dimeric structures during cell culture assays (Figures 8 and S7) and to enter cells intact through passive diffusion.^[9]

Part of the reason for the higher toxicity of **2a,b** and **5** in blood-derived and mesenchymal-like cells over epithelial cells and fibroblasts (Figure 7 and Table 2) is related to variations in

membrane permeability,^[62] which is likely to lead to different rates of cellular Ru uptake and efflux in various cell types. However, this factor does not account for the higher activity of **5** compared with **2a,b** in MDA-MB-231 cells (No. 3 in Figure 7, and Figure 8a,c), since its accumulation in this cell line was lower (Figure 9). Another consideration is the difference in cellular thiol concentrations in various cell types,^[26] since **2a,b** and **5** are likely to act through catalytic cellular thiol depletion,^[28] similarly to other hydrolytically stable Ru(II) arene complexes.^[21, 27] MDA-MB-231 cells are more susceptible to cellular thiol oxidation compared with MCF-7 cells.^[63] Still, if **5** was a more efficient redox catalyst than **2a,b**, it would show consistently higher activity across the panel of cell lines, which was not the case (Figure 7). The mechanisms behind the unusual selectivity of **5** in MDA-MB-231 cells (Figures 7 and 8) will require further investigation with the use of more advanced in vitro models, including hypoxic environment and three-dimensional cell culture systems.^[64]

While the search for new metal-based anti-cancer drugs has long been focused on highly cytotoxic compounds,^[21] the current emphasis is on the selectivity and low systemic toxicity.^[29] Deliberate choice of moderately active but less toxic compounds was behind the clinical success of some established anti-cancer drugs, such as histone deacetylase inhibitors.^[65] In addition, the only Ru complex that was so far successful in clinical trials, IT-139 (or NKP-1339, Figure 1),^[14, 15] showed weak to moderate anti-proliferative activities in cell culture assays (typical IC_{50} values, 20–100 μM Ru after 96 h treatment).^[16] In this respect, **5** can provide an attractive lead in the search of compounds that selectively target more aggressive cancer cells.^[3] Unusually high stability of **5** in biological media for a metal complex (Figures 8 and S7),^[9] particularly compared with the previously studied potentially anti-metastatic Ru complexes such as NAMI-A,^[4, 10] is likely to reduce the probability of side effects that hampered the clinical use of this and other metal anti-cancer drugs.^[6, 11]

Conclusions

We have synthesized and characterized a new series of Ru(II) sulfidocarboxylato complexes of general formula $[\text{Ru}(\rho\text{-cymene})\text{L}]_2$ from a series of α - and β -mercaptocarboxylic acids (L-H₂). Of the twelve Ru(II)-arene thiocarboxylato complexes synthesized, **1a**, **2b**, **3b**, **4a**, **5**, and **6** were amenable to single crystal diffraction studies. The solid state structures of the six complexes revealed isostructural dimeric compositions in which the parent ligand has been doubly deprotonated at the thiol and hydroxyl functionalities allowing O,S-chelation to the Ru(II) metal center.

The cytotoxicity of complexes **1-7** in cultured human cancer cell lines was determined by real-time observations with an IncuCyte Zoom imaging system and in standard MTT assays. In general, the particular activities of these complexes appear to be highly structure dependant. Three of the complexes (**2a,b** and **5**), all of which contain a phenyl substituent in the ligand, showed promising anti-proliferative activities. Complex **5**, $[\text{Ru}(\rho\text{-cymene})(\text{MPP})_2]$, showed moderate but remarkably selective activity in highly invasive MDA-MB-231 cells ($IC_{50} = 39 \pm 4 \mu\text{M}$

FULL PAPER

Ru). **5** induced apoptosis and cell death in MDA-MB-231 cells after 24 h incubation with 50 μ M Ru, but had no effect in A549 (human lung cancer, epithelial) cells under the same conditions. By contrast, **2a** and **b** showed moderate anti-proliferative activity, but no apoptosis, in either cell line. Given the high selectivity of **5** towards highly invasive, mesenchymal-like MDA-MB-231 cells over many common epithelial and fibroblast cells, shows this is an important lead complex for further pre-clinical studies. The choice of ligand has a significant effect on anti-cancer activities and from the promising results in this study, these Ru(II) sulfidocarboxylate complexes warrant further investigation and may emerge one day as new cancer treatment candidates.

Experimental Section

Synthesis and Characterization of 1-7. Unless preparative details are included, solvents and reagents were purchased from commercial suppliers; Sigma Aldrich and ThermoFischer Scientific. Proton (^1H NMR) and carbon magnetic resonance (^{13}C NMR) spectra were recorded on a Bruker AV400 spectrometer at 400 MHz and 100 MHz respectively. Chemical shifts are quoted in parts per million (δ /ppm) and are referenced to the residual solvent peak. Infrared spectroscopy measurements were carried out with a Cary 630 FTIR in the range of 4000-500 cm^{-1} . HPLC purification was conducted using an Agilent Technologies 1260 Infinity Preparative pump with a 1260 DAD VL UV detector (280 nm) on a Phenomenex Onyx Monolithic 100 x 10 mm C_{18} column. The mobile phase was a mixture of MilliQ water and analytical grade methanol using either isocratic conditions or a linear gradient over 15 minutes and a flow rate of 4 mL/min. Mass spectrometry was performed on a Micromass Platform QMS spectrometer with an electrospray source and cone voltage of 35 eV. Melting points were obtained using a Stuart Scientific SMP 3 melting point machine.

(Full experimental details for the synthesis of α - and β -mercaptocarboxylic acids can be found in the Supporting Information).

Preparation of [Ru(*p*-cymene) L] $_2$ complexes: General procedure. To a solution of [RuCl $_2$ (*p*-cymene) $_2$ (1 equiv.) in methanol was added the α/β -mercaptocarboxylic acid (2.5 equiv.) and excess triethylamine (6 equiv.) The solution was stirred at reflux for 1 h before being concentrated under *vacuo*. The resulting crude material was first purified by silica gel column chromatography to remove bulk impurities (SiO_2 , 100% DCM – 20% methanol/DCM), before being further purified using reverse phase prep-HPLC (C18 column Phenomenex Monolithic). Analysis by MS identified fractions that contained the desired compound.

[Ru(*p*-cymene)(TLA)] $_2$ (1a**):** ^1H NMR (400 MHz, Methanol- d_4) δ 5.76 (d, J = 6.9 Hz, 1H), 5.42 (d, J = 5.7 Hz, 1H), 5.36 (d, J = 6.2 Hz, 1H), 5.08 (d, J = 7.0 Hz, 1H), 3.65 (q, J = 7.2 Hz, 1H), 2.77 (sept, J = 6.9 Hz, 1H), 2.11 (s, 3H), 1.52 (d, J = 7.3 Hz, 3H), 1.33 (d, J = 6.9 Hz, 4H), 1.28 (d, J = 7.0 Hz, 3H). ^{13}C NMR (101 MHz, Methanol- d_4) δ 187.8, 107.6, 97.8, 88.6, 88.1, 86.5, 79.0, 50.9,

32.5, 23.9, 22.3, 20.4, 18.9. IR (film, cm^{-1}): ν = 1609 (C=O), 2924 (C-H), 2959 (C-H). MS (ESI) calculated for $\text{C}_{26}\text{H}_{36}\text{O}_4\text{Ru}_2\text{S}_2$: 680.0 (M + H) $^+$, 703.0 (M + Na) $^+$. Yield: 67%. HPLC conditions: isocratic (40% methanol). Melting point: 141 $^\circ\text{C}$ (dec.).

[Ru(*p*-cymene)(TLA)] $_2$ (1b**):** ^1H NMR (400 MHz, Methanol- d_4) δ 5.47 (td, J = 6.7, 1.5 Hz, 2H), 5.34 – 5.26 (m, 2H), 3.06 (q, J = 7.7 Hz, 1H), 2.84 (sept, J = 6.9 Hz, 1H), 2.14 (s, 3H), 1.35 – 1.25 (m, 9H). ^{13}C NMR (101 MHz, Methanol- d_4) δ 187.9, 108.4, 102.2, 87.7, 86.5, 86.2, 83.9, 41.7, 31.9, 23.1, 22.9, 20.4, 18.3. IR (film, cm^{-1}): ν = 1620 (C=O), 2922 (C-H), 2961 (C-H). MS (ESI) calculated for $\text{C}_{26}\text{H}_{36}\text{O}_4\text{Ru}_2\text{S}_2$: 703.0 (M + Na) $^+$. Yield: 11%. HPLC conditions: isocratic (52.5% methanol). Melting point: 133 $^\circ\text{C}$ (dec.).

[Ru(*p*-cymene)(MPA)] $_2$ (2a**):** ^1H NMR (400 MHz, Methanol- d_4) δ 7.38 – 7.34 (m, 4H), 7.28 (ddt, J = 6.6, 5.2, 2.6 Hz, 1H), 5.14 – 5.09 (m, 2H), 5.03 (dd, J = 5.6, 1.5 Hz, 1H), 4.81 (s, 13H), 3.36 (dd, J = 10.7, 3.5 Hz, 2H), 3.09 (dd, J = 13.7, 3.5 Hz, 1H), 2.68 (dd, J = 13.8, 10.7 Hz, 1H), 2.50 (sept, J = 6.9 Hz, 1H), 2.00 (s, 3H), 1.13 (d, J = 6.9 Hz, 6H). ^{13}C NMR (101 MHz, Methanol- d_4) δ 186.9, 140.9, 131.0, 129.3, 127.8, 108.1, 102.0, 87.1, 87.1, 86.2, 83.4, 40.4, 31.6, 23.0, 22.9, 18.4. IR (film, cm^{-1}): ν = 1605 (C=O), 2929 (C-H), 2960 (C-H). MS (ESI) calculated for $\text{C}_{38}\text{H}_{44}\text{O}_4\text{Ru}_2\text{S}_2$: 831.0 (M + H) $^+$, 852.9 (M + Na) $^+$. Yield: 46%. HPLC conditions: gradient (60% - 75% methanol). Melting point: 114 $^\circ\text{C}$ (dec.).

[Ru(*p*-cymene)(MPA)] $_2$ (2b**):** ^1H NMR (400 MHz, Methanol- d_4) δ 7.39 – 7.34 (m, 4H), 7.30 – 7.25 (m, 1H), 5.12 (td, J = 5.8, 5.3, 1.2 Hz, 2H), 5.03 (d, J = 5.2 Hz, 1H), 4.82 (d, J = 5.6 Hz, 6H), 3.36 (dd, J = 10.7, 3.5 Hz, 1H), 3.09 (dd, J = 13.7, 3.5 Hz, 1H), 2.68 (dd, J = 13.7, 10.7 Hz, 1H), 2.50 (sept, J = 7.0 Hz, 1H), 2.00 (s, 3H), 1.13 (d, J = 6.9 Hz, 6H). ^{13}C NMR (101 MHz, Methanol- d_4) δ 186.9, 140.9, 131.0, 129.3, 127.8, 108.1, 102.0, 87.1, 87.1, 86.2, 83.4, 49.7, 49.5, 49.3, 49.1, 48.4, 40.4, 31.6, 23.0, 22.9, 18.4. IR (film, cm^{-1}): ν = 1606 (C=O), 2927 (C-H), 2962 (C-H). MS (ESI) calculated for $\text{C}_{38}\text{H}_{44}\text{O}_4\text{Ru}_2\text{S}_2$: 831.0 (M + H) $^+$, 852.9 (M + Na) $^+$. Yield: 46%. HPLC conditions: gradient (60% - 75% methanol). Melting point: 114 $^\circ\text{C}$ (dec.).

[Ru(*p*-cymene)(MMA)] $_2$ (3a**):** ^1H NMR (400 MHz, Methanol- d_4) δ 5.47 (d, J = 7.2 Hz, 1H), 5.33 (d, J = 7.4 Hz, 1H), 5.26 (d, J = 7.1 Hz, 1H), 5.14 (d, J = 7.3 Hz, 1H), 3.17 (d, J = 4.1 Hz, 1H), 2.82 (sept, J = 6.9 Hz, 1H), 2.28 (s, 3H), 2.20 (pd, J = 6.8, 4.2 Hz, 1H), 1.31 (dd, J = 6.9, 1.6 Hz, 6H), 1.07 (d, J = 6.9 Hz, 3H), 0.92 (d, J = 6.7 Hz, 3H). ^{13}C NMR (101 MHz, Methanol- d_4) δ 187.7, 108.4, 101.4, 88.6, 87.9, 82.1, 51.4, 32.7, 32.0, 23.4, 23.1, 21.3, 19.2, 18.6. IR (film, cm^{-1}): ν = 1601 (C=O), 2927 (C-H), 2957 (C-H). MS (ESI) calculated for $\text{C}_{30}\text{H}_{44}\text{O}_4\text{Ru}_2\text{S}_2$: 735.9 (M + H) $^+$, 758.0 (M + Na) $^+$. Yield: 48%. HPLC conditions: gradient (60% - 70% methanol). Melting point: 146 $^\circ\text{C}$ (dec.).

[Ru(*p*-cymene)(MMA)] $_2$ (3b**):** ^1H NMR (400 MHz, Methanol- d_4) δ 5.46 (d, J = 7.1 Hz, 1H), 5.33 (d, J = 7.4 Hz, 1H), 5.26 (d, J = 7.2 Hz, 1H), 5.14 (d, J = 7.3 Hz, 1H), 3.17 (d, J = 4.1 Hz, 1H), 2.82 (sept, J = 7.0 Hz, 1H), 2.28 (s, 3H), 2.20 (pd, J = 6.8, 4.1 Hz, 1H), 1.31 (dd, J = 6.9, 1.5 Hz, 6H), 1.07 (d, J = 6.9 Hz, 3H), 0.92 (d, J = 6.8 Hz, 3H). ^{13}C NMR (101 MHz, Methanol- d_4) δ 187.7, 108.4,

FULL PAPER

101.4, 88.6, 87.9, 82.1, 51.4, 32.7, 32.0, 23.4, 23.1, 21.3, 19.2, 18.6. IR (film, cm^{-1}): $\nu = 1601$ (C=O), 2927 (C-H), 2955 (C-H). MS (ESI) calculated for $\text{C}_{30}\text{H}_{44}\text{O}_4\text{Ru}_2\text{S}_2$: 735.9 (M + H)⁺, 758.0 (M + Na)⁺. Yield: 52%. HPLC conditions: gradient (60% - 70% methanol). Melting point: 147 °C (dec.).

[Ru(*p*-cymene)(MBA)]₂ (4a): ¹H NMR (400 MHz, Methanol-*d*₄) δ 5.59 (d, *J* = 5.7 Hz, 1H), 5.41 (d, *J* = 6.2 Hz, 1H), 5.29 (d, *J* = 6.2 Hz, 1H), 4.96 (d, *J* = 5.7 Hz, 1H), 3.17 (ddd, *J* = 11.7, 6.8, 3.6 Hz, 1H), 2.74 – 2.66 (m, 2H), 2.46 (dd, *J* = 13.2, 11.6 Hz, 1H), 2.15 (s, 3H), 1.38 (d, *J* = 6.8 Hz, 3H), 1.29 (dd, *J* = 15.1, 6.9 Hz, 6H). ¹³C NMR (101 MHz, Methanol-*d*₄) δ 182.8, 107.9, 98.6, 88.2, 88.2, 85.9, 79.6, 48.9, 40.5, 32.0, 25.1, 23.4, 22.3, 18.6. IR (film, cm^{-1}): $\nu = 1579$ (C=O), 2918 (C-H), 2960 (C-H). MS (ESI) calculated for $\text{C}_{28}\text{H}_{40}\text{O}_4\text{Ru}_2\text{S}_2$: 707.9 (M + H)⁺, 730.9 (M + Na)⁺. Yield: 66%. HPLC conditions: gradient (40% - 60% methanol). Melting point: 112 °C (dec.).

[Ru(*p*-cymene)(MBA)]₂ (4b): ¹H NMR (400 MHz, Methanol-*d*₄) δ 5.36 (dd, *J* = 8.3, 5.9 Hz, 2H), 5.22 (d, *J* = 6.0 Hz, 1H), 5.17 (d, *J* = 5.8 Hz, 1H), 2.92 (sept, *J* = 6.9 Hz, 1H), 2.76 (ddp, *J* = 10.3, 6.8, 3.5 Hz, 1H), 2.47 – 2.32 (m, 2H), 2.23 (s, 3H), 1.32 (dd, *J* = 6.9, 6.2 Hz, 6H), 1.17 (d, *J* = 6.8 Hz, 3H). ¹³C NMR (101 MHz, Methanol-*d*₄) δ 183.2, 111.3, 102.7, 86.8, 86.7, 85.6, 84.3, 47.8, 31.4, 29.0, 23.9, 23.0, 22.6, 18.0. IR (film, cm^{-1}): $\nu = 1604$ (C=O), 2916 (C-H), 2959 (C-H). MS (ESI) calculated for $\text{C}_{28}\text{H}_{40}\text{O}_4\text{Ru}_2\text{S}_2$: 707.9 (M + H)⁺, 730.9 (M + Na)⁺. Yield: 27%. HPLC conditions: gradient (50% - 65% methanol). Melting point: 123 °C (dec.).

[Ru(*p*-cymene)(MPP)]₂ (5): ¹H NMR (400 MHz, Methanol-*d*₄) δ 7.55 – 7.47 (m, 2H), 7.34 (t, *J* = 7.4 Hz, 2H), 7.28 – 7.23 (m, 1H), 5.33 – 5.27 (m, 2H), 5.17 (d, *J* = 5.2 Hz, 1H), 5.11 (d, *J* = 4.9 Hz, 1H), 3.90 (dd, *J* = 13.1, 1.4 Hz, 1H), 3.05 (dd, *J* = 15.0, 13.1 Hz, 1H), 2.67 – 2.57 (m, 2H), 2.02 (s, 3H), 1.14 (d, *J* = 6.9 Hz, 3H), 1.01 (d, *J* = 6.9 Hz, 3H). ¹³C NMR (101 MHz, Methanol-*d*₄) δ 183.5, 144.8, 129.6, 129.3, 128.1, 111.8, 104.3, 86.4, 86.0, 85.5, 84.5, 46.8, 35.9, 31.5, 23.1, 22.3, 17.8. IR (film, cm^{-1}): $\nu = 1641$ (C=O), 2998 (C-H). MS (ESI) calculated for $\text{C}_{38}\text{H}_{46}\text{O}_4\text{Ru}_2\text{S}_2$: 832.0 (M + H)⁺, 854.9 (M + Na)⁺. Yield: 43%. HPLC conditions: gradient (65% - 75% methanol). Melting point: 134 °C (dec.).

[Ru(*p*-cymene)(MMPA)]₂ (6): ¹H NMR (400 MHz, Methanol-*d*₄) δ 7.44 – 7.41 (m, 2H), 6.91 – 6.88 (m, 2H), 5.30 – 5.27 (m, 2H), 5.14 (d, *J* = 5.7 Hz, 1H), 5.10 (d, *J* = 5.7 Hz, 1H), 3.84 (dd, *J* = 13.2, 1.5 Hz, 1H), 3.81 (s, 3H), 3.02 (dd, *J* = 15.0, 13.1 Hz, 1H), 2.65 – 2.60 (m, 2H), 2.03 (s, 3H), 1.15 (d, *J* = 6.9 Hz, 3H), 1.04 (d, *J* = 6.9 Hz, 3H). ¹³C NMR (101 MHz, Methanol-*d*₄) δ 183.7, 160.3, 136.7, 130.3, 115.0, 111.7, 104.2, 86.4, 85.8, 85.4, 84.5, 55.8, 47.0, 35.4, 31.4, 23.1, 22.4, 17.8. IR (film, cm^{-1}): $\nu = 1599$ (C=O), 2909 (C-H), 2955 (C-H). MS (ESI) calculated for $\text{C}_{40}\text{H}_{48}\text{O}_6\text{Ru}_2\text{S}_2$: 892.1 (M + H)⁺, 915.0 (M + Na)⁺. Yield: 52%. HPLC conditions: gradient (65% - 75% methanol). Melting point: 138 °C (dec.).

[Ru(*p*-cymene)(TSA)]₂ (7a): All analytical data, such as NMR spectra and MP, were consistent with the literature reported values for compound **7a**.^[34] ¹H NMR (400 MHz, Chloroform-*d*) δ

8.14 (dd, *J* = 7.7, 1.5 Hz, 1H), 7.67 (dd, *J* = 7.7, 1.0 Hz, 1H), 7.39 (td, *J* = 7.5, 1.2 Hz, 1H), 7.24 (dd, *J* = 7.6, 1.7 Hz, 1H), 5.10 (d, *J* = 5.9 Hz, 1H), 4.82 – 4.73 (m, 2H), 4.62 (d, *J* = 5.6 Hz, 1H), 2.51 (sept, *J* = 6.9 Hz, 1H), 1.84 (s, 3H), 1.15 (d, *J* = 7.0 Hz, 3H), 0.86 (d, *J* = 6.8 Hz, 3H). ¹³C NMR (101 MHz, Chloroform-*d*) δ 171.6, 139.4, 133.1, 132.3, 128.9, 128.5, 107.5, 99.6, 84.0, 83.4, 83.3, 83.3, 29.9, 23.3, 21.3, 17.7. IR (film, cm^{-1}): $\nu = 1587$ (C=O), 2926 (C-H), 2971 (C-H). MS (ESI) calculated for $\text{C}_{34}\text{H}_{36}\text{O}_4\text{Ru}_2\text{S}_2$: 777.0 (M + H)⁺, 800.0 (M + Na)⁺. Yield: 65%. HPLC conditions not required.

[Ru(*p*-cymene)(TSA)]₂ (7b): ¹H NMR (400 MHz, Methanol-*d*₄) δ 8.19 – 8.15 (m, 1H), 7.60 – 7.56 (m, 1H), 7.43 – 7.37 (m, 2H), 5.52 (d, *J* = 5.9 Hz, 1H), 5.40 (dd, *J* = 12.1, 5.9 Hz, 2H), 5.28 (d, *J* = 6.0 Hz, 1H), 3.35 (s, 1H), 2.12 (sept, *J* = 6.9 Hz, 1H), 1.60 (s, 3H), 0.85 (d, *J* = 6.9 Hz, 3H), 0.67 (d, *J* = 6.8 Hz, 3H). ¹³C NMR (101 MHz, Methanol-*d*₄) δ 173.6, 142.7, 137.6, 136.0, 131.0, 129.0, 128.9, 108.9, 101.2, 86.7, 86.3, 85.2, 85.1, 31.6, 23.4, 21.4, 17.8. IR (film, cm^{-1}): 2961 (C-H). MS (ESI) calculated for $\text{C}_{34}\text{H}_{36}\text{O}_4\text{Ru}_2\text{S}_2$: 800.0 (M + Na)⁺. Yield: 12%. HPLC conditions: gradient (50% - 80% methanol). Melting point: 258 °C (dec.).

KP1019 was synthesized and characterized as described previously.^[52]

X-Ray Crystallography. Crystallographic data of compounds **1-3** was collected at the MX1 beamline at the Australian Synchrotron, Melbourne, Victoria, Australia ($\lambda = 0.71070$ Å). All data were collected at 100 K, maintained using an open flow of nitrogen. The software used for data collection and reduction of the data were Bluice and XDS. Crystallographic data for complexes **5** and **6** were obtained on a Bruker X8 APEXII CCD diffractometer equipped with an OXFORD Cryosystems 700 Cryostream and cooled to 123(1) K. Data were collected with monochromatic (graphite) Mo K α radiation ($\lambda = 0.71073$ Å) and processed using the Bruker Apex2 v2012.2.0 software; Lorentz, polarization and absorption corrections (multi-scan – SADABS) were applied. Crystallographic data for compound **4a** were obtained on Rigaku Synergy S diffractometer Mo K α radiation ($\lambda = 0.71073$ Å) HYPIX_6000HE. Compounds **1-6** were solved and refined with SHELX-97. All non-hydrogen atoms were refined with anisotropic thermal parameters unless otherwise indicated and hydrogen atoms were placed in calculated positions using a riding model with C-H = 0.95-0.98 Å and Uiso(H) = xUiso(C), x = 1.2 or 1.5. Data for **1a**, **2b**, **3b**, **4a**, **5** and **6** has been deposited with the Cambridge Crystallographic Database with CCDC number 1046084, 1046085, 1046086, 1901567, 1901574 and 1046087 respectively.

Crystal Data for 1a: $\text{C}_{26}\text{H}_{36}\text{O}_6\text{Ru}_2\text{S}_2$; Mr = 710.81; triclinic; space group: P-1; *a* = 9.167 (18), *b* = 10.208 (2), *c* = 15.506 (3); α = 83.32 (3); β = 87.39 (3); γ = 73.83 (3); *V* = 1384.0(5) Å³; *Z* = 2, reflections collected/unique: 6012/6012 (*R*_{int} = 0.0327); *R*₁ values (*I* > 2 σ (*I*)) = 0.0405; *wR*(*F*²) values (*I* > 2 σ (*I*)) = 0.1091; *R*₁ values (all data) = 0.0417; *wR*(*F*²) values (all data) = 0.1102; GOF = 1.052.

FULL PAPER

Crystal Data for 2b: $C_{30}H_{44}O_7Ru_2S_2$; Mr = 782.91; monoclinic; space group: P21/c; $a = 13.682$ (3), $b = 15.375$ (3), $c = 17.054$ (3); $\beta = 110.61$ (3); $V = 3357.8$ (12) Å³; $Z = 4$, reflections collected/unique: 55310/7958 ($R_{int} = 0.0738$); R_1 values ($I > 2\sigma(I)$) = 0.0469; $wR(F^2)$ values ($I > 2\sigma(I)$) = 0.1171; R_1 values (all data) = 0.0572; $wR(F^2)$ values (all data) = 0.1227; GOF = 1.022.

Crystal Data for 3b: $C_{42}H_{54}O_6Ru_2S_2$; Mr = 921.11; triclinic; space group: P-1; $a = 8.8340$ (18), $b = 10.281$ (2), $c = 12.880$ (3); $\alpha = 72.96$ (3); $\beta = 78.96$ (3); $\gamma = 65.53$ (3); $V = 1014.6$ (4) Å³; $Z = 1$, reflections collected/unique: 19968/5246 ($R_{int} = 0.0322$); R_1 values ($I > 2\sigma(I)$) = 0.0521; $wR(F^2)$ values ($I > 2\sigma(I)$) = 0.1457; R_1 values (all data) = 0.0552; $wR(F^2)$ values (all data) = 0.1474; GOF = 1.145.

Crystal Data for 4a: $C_{28}H_{46}O_7Ru_2S_2$; Mr = 760.91; triclinic; space group: P-1; $a = 10.9622$ (2), $b = 11.3748$ (3), $c = 13.5843$ (4); $\alpha = 69.997$ (2); $\beta = 81.661$ (2); $\gamma = 80.084$ (2); $V = 1561.10$ (7) Å³; $Z = 2$, reflections collected/unique: 47943/6475 ($R_{int} = 0.0896$); R_1 values ($I > 2\sigma(I)$) = 0.0666; $wR(F^2)$ values ($I > 2\sigma(I)$) = 0.1609; R_1 values (all data) = 0.0777; $wR(F^2)$ values (all data) = 0.1677; GOF = 1.097.

Crystal Data for 5: $C_{38}H_{44}O_4Ru_2S_2$; Mr = 831.02; triclinic; space group: P-1; $a = 8.8674$ (9), $b = 10.1893$ (9), $c = 10.3615$ (9); $\alpha = 72.345$ (3); $\beta = 89.989$ (4); $\gamma = 65.774$ (3); $V = 805.17$ (12) Å³; $Z = 1$, reflections collected/unique: 20079/4976 ($R_{int} = 0.0832$); R_1 values ($I > 2\sigma(I)$) = 0.0447; $wR(F^2)$ values ($I > 2\sigma(I)$) = 0.0775; R_1 values (all data) = 0.0641; $wR(F^2)$ values (all data) = 0.0857; GOF = 1.075.

Crystal Data for 6: $C_{44}H_{60}O_8Ru_2S_2$; Mr = 983.21; triclinic; space group: P-1; $a = 9.2472$ (5), $b = 11.2364$ (6), $c = 11.6790$ (3); $\alpha = 115.282$ (3); $\beta = 104.523$ (3); $\gamma = 97.263$ (3); $V = 1023.72$ (9) Å³; $Z = 2$, reflections collected/unique: 15961/5867 ($R_{int} = 0.0205$); R_1 values ($I > 2\sigma(I)$) = 0.0208; $wR(F^2)$ values ($I > 2\sigma(I)$) = 0.0479; R_1 values (all data) = 0.0233; $wR(F^2)$ values (all data) = 0.0492; GOF = 1.027.

Stability studies of 1-7 in aqueous media. Electrospray ionization mass spectrometry (ESI-MS) data for 1-7 under biomimetic conditions^{19, 40, 42} were collected on a Bruker amaZon SL spectrometer, using the following parameters: nebulizer pressure, 27.3 psi; spray voltage, 4.5 kV; capillary temperature, 453 K; N₂ flow rate, 4 L min⁻¹; m/z range, 100-2000 (alternating positive and negative ion modes). Analyzed solutions (5.0 μL) were injected into a flow of MeOH (flow rate, 0.30 mL min⁻¹). Acquired spectra were the averages of 100-200 scans (scan time, 10 ms). Solutions for mass spectrometry were prepared by diluting stock solutions of 1-7 (1.0 μL of 2-20 mM in DMF) with aqueous NH₄HCO₃ (350 μL of 10 mM, pH 7.5). The resultant solutions were stored for several hours or days at 295 K, then mixed with MeOH (50 μL) immediately prior to collecting the ESI-MS data. Simulations of the mass spectra were performed using IsoPro software.^[66]

Cell culture and MTT proliferation assays. Pre-sterilized media and sterile plasticware used in cell culture were purchased from Life Technologies Australia. Cell lines (listed in Table 2) were purchased from American Type Culture Collection (ATCC, www.atcc.org), or European Collection of Authenticated Cell Cultures (ECACC, www.phe-culturecollection.org.uk). The cells were cultured using standard techniques^[67] in Advanced DMEM (Thermo Fisher 12491-015), supplemented with L-glutamine (2.0 mM), antibiotic-antimycotic mixture (100 U mL⁻¹ penicillin, 100 mg mL⁻¹ streptomycin and 0.25 mg mL⁻¹ amphotericin B) and fetal calf serum (FCS; heat-inactivated; 2 % vol). For proliferation experiments, cells were seeded in 96-well plates in 0.10 mL medium per well, and incubated overnight (310 K, 5% CO₂) before replacing the growth medium with fully supplemented medium containing Ru complexes. Non-adherent cells (Nos. 1 and 2, Table 2) were seeded at 1.0×10⁴ viable cells per well in round-bottom plates, while adherent cells (Nos. 3-15, Table 2) were seeded at 1.0×10³ viable cells per well in flat-bottom plates. Cell counting and viability tests were performed using Countess automatic counter (Thermo Fisher) with chamber slides and Trypan blue dye.^[67]

Stock solutions of the complexes were 1-12 mM Ru in DMSO (preliminary experiments, Figure S6), or 20 mM Ru in DMF (main experiments, Figures 7 and S7). These solutions were stable for at least a month when stored in the dark at 295 K (verified by ESI-MS, Figure S8). Unless stated otherwise, stock solutions were diluted 100-400-fold with fully supplemented cell culture medium immediately before cell treatments. All treatments contained the same amount of organic solvent (0.25% vol. DMF or 1.0% vol. DMSO), which was also added to the medium in control wells. At these concentrations, the organic solvents did not have any significant effect on cell viability over 72-96 h treatments.^[41] Each treatment included six replicate wells and two background wells that contained the same components except the cells. After 72 h incubations (310 K, 5% CO₂), MTT reagent (Sigma M5655) was added (50 μL per well of freshly prepared 2.0 mg mL⁻¹ solution in complete medium), and incubation was continued for 4-6 h. After that, the medium was removed, the blue formazan crystals were dissolved in 0.10 mL per well of DMSO, and the absorbance at 600 nm was measured using Victor V3 plate reader.^[45] Calculation of IC₅₀ values and statistical analysis of the results were performed using Origin software.^[68] For all the cell assays, consistent results were obtained in at least two independent experiments, using different passages of cells and different stock solutions of the treatment compounds.

IncuCyte proliferation and cytotoxicity assays. MDA-MB-231 and A549 cells (Table 2) were seeded at 2.0×10³ cells per well in flat-bottom 96-well plates (Corning 3599) and left to attach overnight (310 K, 5% CO₂), after which the growth medium was replaced with fully supplemented treatment medium containing Ru complexes (50 μM Ru), Caspase 3/7 reagent (3.0 μM)^[50] and Cytotox Red (0.30 μM).^[51] The plates were placed into an IncuCyte Zoom imaging system^[39] that was maintained at 310 K, 5% CO₂, and phase contrast and fluorescent images were collected every 2 h for 80-100 h, using x10 objective. Green and red fluorescence acquisition times were 0.40 s and 0.80 s,

FULL PAPER

respectively. Image analyses were performed with InCuCyte software,^[39] using the following parameters: cell over background threshold, 1.0; minimal object size, 300 μm^2 ; green threshold, 2.0; red threshold, 0.5; 5% of green fluorescence removed from the red channel. Further analysis and plotting of InCuCyte data was performed using Origin software.^[68]

Measurements of Ru in cell culture media and cell lysates.

Analyses were performed by graphite furnace atomic absorption spectrometry (GFAAS), using an Agilent Technologies series 200 spectrometer, equipped with Zeeman background correction. Standard Ru solution (Aldrich 207446) was diluted with 0.10 M HCl (prepared from 35% aqueous solution, trace pure grade, Merck Cat. No. 1.15186) for calibration (0-500 ppb Ru). Aliquots (50 μL) of Ru-containing media from the cell assays were diluted to 1.0 mL with 0.10 M HCl and left overnight at 295 K before the GFAAS measurements.

Cellular Ru uptake was measured following our published method.^[40, 52, 69] Cell treatments were performed in triplicate in six-well plates, either by growing MDA-MB-231 or A549 cells to ~80% confluence and then incubating them with 50 μM Ru for 4 h (Figure 9a), or seeding 1.0×10^5 viable cells per well and growing them to near-confluence for 72 h in the presence of 20 μM Ru (Figure 9b). After the treatments, the medium was removed, the cell layers were washed three times with PBS, collected by trypsinization, pelleted (3 min at 600 g), washed again with PBS, and digested with 0.10 mL of 0.10 M NaOH by pipetting up and down and storing overnight at 277 K. Trypsinization and washing of cell pellets was used to remove Ru that was adsorbed on plastic ware and on the cell surface.^[70] Since the resultant lysate was viscous, an aliquot (10 μL) was taken with a positive displacement pipette, diluted 10-fold with 0.10 M NaOH, and used for protein determination. For this, aliquots of the dilute lysate ($3 \times 10 \mu\text{L}$) were mixed with Bradford reagent (90 μL , Sigma B6916), and the absorbance at 600 nm was measured using a Victor V3 plate reader. Freshly prepared BSA solutions in 0.10 M NaOH

(0.10-1.0 mg mL^{-1}) were used for calibration. The remaining undiluted lysate was brought to 1.0 mL with 0.10 M HCl, left overnight at 295 K, centrifuged for 2 min at 16,000 g to remove denatured protein, and used for GFAAS measurements. The results were presented in nmol Ru per mg protein (Figure 9).

Acknowledgements

Financial support for this work was provided by Australian Research Council (ARC) grants to PAL for an ARC Senior Research Associate position for AL (DP130103566, DP160104172). The authors acknowledge the facilities and the scientific and technical assistance of the Mass Spectrometry Facility, School of Chemistry, University of Sydney (Nicholas Proschogo); Australian Microscopy & Microanalysis Research Facility at the Australian Centre for Microscopy & Microanalysis at the University of Sydney (Minh Huynh and Ellie Kable) for the use of cell culture laboratory; and Molecular Biology Facility of the Bosch Institute, University of Sydney (Donna Lai and Sheng Hua) for the use of InCuCyte. The authors also acknowledge the scientific and technical assistance of Mr. Phillip Holt with HPLC at Monash University.

Keywords: Anti-cancer agents • Anti-metastatic • Apoptosis • Breast cancer • Ruthenium • Selectively cytotoxic

FULL PAPER

- [1] K. R. Fischer, A. Durrans, S. Lee, J. Sheng, F. Li, S. T. C. Wong, H. Choi, T. El Rayes, S. Ryu, J. Troeger, R. F. Schwabe, L. T. Vahdat, N. K. Altorki, V. Mittal, D. Gao, *Nature (London, U. K.)* **2015**, *527*, 472-476.
- [2] R. L. Anderson, T. Balasas, J. Callaghan, R. C. Coombes, J. Evans, J. A. Hall, S. Kinrade, D. Jones, P. S. Jones, R. Jones, J. F. Marshall, M. B. Panico, J. A. Shaw, P. S. Steeg, M. Sullivan, W. Tong, A. D. Westwell, J. W. A. Ritchie, U. K. on behalf of the Cancer Research. Cancer Therapeutics, *Nat. Rev. Clin. Oncol.* **2018**, *16*, 185-204.
- [3] P. Gautam, L. Karhinen, A. Sz wajda, J. S. Kumar, B. Yadav, T. Aittokallio, K. Wennerberg, *Mol. Cancer* **2016**, *15*, article 34.
- [4] G. Sava, R. Gagliardi, M. Cocchietto, K. Clerici, I. Capozzi, M. Marrella, E. Alessio, G. Mestroni, R. Milanino, *Pathol. Oncol. Res.* **1998**, *4*, 30-36.
- [5] A. Bergamo, A. Masi, P. J. Dyson, G. Sava, *Int. J. Oncol.* **2008**, *33*, 1281-1289.
- [6] D. M. Cheff, M. D. Hall, *J. Med. Chem.* **2017**, *60*, 4517-4532.
- [7] J. Reedijk, *Platinum Met. Rev.* **2008**, *52*, 2-11.
- [8] A. Levina, A. Mitra, P. A. Lay, *Metalomics* **2009**, *1*, 458-470.
- [9] A. Levina, D. C. Crans, P. A. Lay, *Coord. Chem. Rev.* **2017**, *352*, 473-498.
- [10] M. Liu, Z. J. Lim, Y. Y. Gwee, A. Levina, P. A. Lay, *Angew. Chem., Int. Ed.* **2010**, *49*, 1661-1664, S1661/1661-S1661/1669.
- [11] E. Alessio, *Eur. J. Inorg. Chem.* **2017**, *2017*, 1549-1560.
- [12] R. F. S. Lee, S. Escrig, C. Maclachlan, G. W. Knott, A. Meibom, G. Sava, P. J. Dyson, *Int. J. Mol. Sci.* **2017**, *18*, article 1869.
- [13] E. Alessio, L. Messori, *Met. Ions Life Sci.* **2018**, *18*, 141-170.
- [14] H. A. Burris, J. C. Bendell, J. Infante, S. F. Jones, D. R. Spiegel, S. Bakewell, G. J. Weiss, R. K. Ramanathan, H. D. Von, A. Ogden, *ESMO Open* **2016**, *1*, e000154.
- [15] R. Trondl, P. Heffeter, C. R. Kowol, M. A. Jakupc, W. Berger, B. K. Keppler, *Chem. Sci.* **2014**, *5*, 2925-2932.
- [16] L. S. Flocke, R. Trondl, M. A. Jakupc, B. K. Keppler, *Invest. New Drugs* **2016**, *34*, 261-268.
- [17] a) R. E. Aird, J. Cummings, A. A. Ritchie, M. Muir, R. E. Morris, H. Chen, P. J. Sadler, D. I. Jodrell, *British Journal of Cancer* **2002**, *86*, 1652-1657; b) F. Y. Wang, A. Habtemariam, E. P. L. van der Geer, R. Fernandez, M. Melchart, R. J. Deeth, R. Aird, S. Guichard, F. P. A. Fabbiani, P. Lozano-Casal, I. D. H. Oswald, D. I. Jodrell, S. Parsons, P. J. Sadler, *Proceedings of the National Academy of Sciences of the United States of America* **2005**, *102*, 18269-18274.
- [18] A. K. Singh, D. S. Pandey, Q. Xu, P. Braunstein, *Coord. Chem. Rev.* **2014**, *270-271*, 31-56.
- [19] a) A. A. Nazarov, C. G. Hartinger, P. J. Dyson, *J. Organomet. Chem.* **2014**, *751*, 251-260; b) S. K. Singh, D. S. Pandey, *RSC Adv.* **2014**, *4*, 1819-1840; c) L. Biancalana, G. Pampaloni, F. Marchetti, *Chimia* **2017**, *71*, 573-579; d) M. V. Babak, W. H. Ang, *Met. Ions Life Sci.* **2018**, *18*, 171-198.
- [20] G. Suss-Fink, *J. Organomet. Chem.* **2014**, *751*, 2-19.
- [21] J. Furrer, G. Suss-Fink, *Coord. Chem. Rev.* **2016**, *309*, 36-50.
- [22] F. Giannini, J. Furrer, G. Suss-Fink, C. M. Clavel, P. J. Dyson, *J. Organomet. Chem.* **2013**, *744*, 41-48.
- [23] F. Giannini, L. Geiser, L. E. H. Paul, T. Roder, B. Therrien, G. Suss-Fink, J. Furrer, *J. Organomet. Chem.* **2015**, *783*, 40-45.
- [24] A. Koceva-Chyla, K. Matczak, M. P. Hikiusz, M. K. Durka, M. K. Kochel, G. Suess-Fink, J. Furrer, K. Kowalski, *ChemMedChem* **2016**, *11*, 2171-2187.
- [25] D. Muthna, P. Tomsik, R. Havelek, R. Koehlerova, V. Kasilingam, E. Cermakova, D. Stibal, M. Rezacova, G. Suess-Fink, *Anti-Cancer Drugs* **2016**, *27*, 643-650.
- [26] I. Romero-Canelon, M. Mos, P. J. Sadler, *J. Med. Chem.* **2015**, *58*, 7874-7880.
- [27] S. J. Dougan, A. Habtemariam, S. E. McHale, S. Parsons, P. J. Sadler, *Proc. Natl. Acad. Sci. U. S. A.* **2008**, *105*, 11628-11633.
- [28] F. Giannini, G. Suss-Fink, J. Furrer, *Inorg. Chem.* **2011**, *50*, 10552-10554.
- [29] F. Chen, I. Romero-Canelon, J. J. Soldevila-Barreda, J.-I. Song, J. P. C. Coverdale, G. J. Clarkson, J. Kasarkova, A. Habtemariam, M. Wills, V. Brabec, P. J. Sadler, *Organometallics* **2018**, *37*, 1555-1566.
- [30] M. A. Jakupc, V. B. Arion, S. Kapitza, E. Reisner, A. Eichinger, M. Pongratz, B. Marian, N. Graf von Keyserling, B. K. Keppler, *Int. J. Clin. Pharmacol. Ther.* **2005**, *43*, 595-596.
- [31] S. Su, Q. Liu, J. Chen, J. Chen, F. Chen, C. He, D. Huang, W. Wu, L. Lin, W. Huang, J. Zhang, X. Cui, F. Zheng, H. Li, H. Yao, F. Su, E. Song, *Cancer Cell* **2014**, *25*, 605-620.
- [32] N. Tka, J. Kraiem, B. Ben Hassine, *Synthetic Communications* **2013**, *43*, 735-743.
- [33] a) Y. Nai, J. Xu, *Helvetica Chimica Acta* **2013**, *96*, 1355-1365; b) O. Brucher, U. Bergstrasser, H. Kelm, J. Hartung, M. Greb, I. Svoboda, H. Fuess, *Tetrahedron* **2012**, *68*, 6968-6980.
- [34] W. Henderson, B. K. Nicholson, A. G. Oliver, C. E. F. Rickard, *Journal of Organometallic Chemistry* **2001**, *625*, 40-46.
- [35] S. Mirtschin, A. Slabon-Turski, R. Scopelliti, A. H. Velders, K. Severin, *Journal of the American Chemical Society* **2010**, *132*, 14004-14005.
- [36] G. B. Deacon, R. J. Phillips, *Coordination Chemistry Reviews* **1980**, *33*, 227-250.
- [37] a) Q. D. Zhou, T. W. Hambley, B. J. Kennedy, P. A. Lay, *Inorganic Chemistry* **2003**, *42*, 8557-8566; b) J. E. Weder, T. W. Hambley, B. J. Kennedy, P. A. Lay, G. J. Foran, A. M. Rich, *Inorganic Chemistry* **2001**, *40*, 1295-1302; c) A. Levina, R. S. Armstrong, P. A. Lay, *Coordination Chemistry Reviews* **2005**, *249*, 141-160.
- [38] a) M. L. Jaramillo, M. Banville, C. Collins, B. Paul-Roc, L. Bourget, M. O'Connor-McCourt, *Cancer Biol. Ther.* **2008**, *7*, 557-568; b) C.-C. Xu, L.-M. Wu, W. Sun, N. Zhang, W.-S. Chen, X.-N. Fu, *Mol. Med. Rep.* **2011**, *4*, 1007-1015.
- [39] E. Bioscience, Live cell imaging system and data processing system, **2015**.
- [40] A. Levina, A. Wijetunga, R. Kaur, J. T. Koehn, D. C. Crans, P. A. Lay, *Chem. Sci.* **2019**, submitted.
- [41] M. Timm, L. Saaby, L. Moesby, E. W. Hansen, *Cytotechnology* **2013**, *65*, 887-894.
- [42] M. Le, O. Rathje, A. Levina, P. A. Lay, *JBIC, J. Biol. Inorg. Chem.* **2017**, *22*, 663-672.
- [43] A. Levina, P. A. Lay, *Chem. - Asian J.* **2017**, *12*, 1692-1699.
- [44] a) M. Patra, T. Joshi, V. Pierroz, K. Ingram, M. Kaiser, S. Ferrari, B. Spingler, J. Keiser, G. Gasser, *Chem. Eur. J.* **2013**, *19*, 14768-14772; b) M. D. Hall, K. A. Telma, K.-E. Chang, T. D. Lee, J. P. Madigan, J. R. Lloyd, I. S. Goldlust, J. D. Hoeschele, M. M. Gottesman, *Cancer Res.* **2014**, *74*, 3913-3922.
- [45] P. W. Sylvester, *Methods Mol. Biol. (N. Y., NY, U. S. A.)* **2011**, *716*, 157-168.
- [46] T. Mishima, M. Naotsuka, Y. Horita, M. Sato, K. Ohashi, K. Mizuno, *Biochem. Biophys. Res. Commun.* **2010**, *392*, 577-581.
- [47] S. Baribeau, P. Chaudhry, S. Parent, E. Asselin, *PLoS One* **2014**, *9*, e86987/86981-e86987/86912, 86912 pp.
- [48] M. Soundararajan, S. Kannan, *J. Cell. Physiol.* **2018**, *233*, 9099-9109.
- [49] a) A. K. Godwin, A. Meister, P. J. O'Dwyer, C. S. Huang, T. C. Hamilton, M. E. Anderson, *Proc. Natl. Acad. Sci. U. S. A.* **1992**, *89*, 3070-3074; b) J. Liang, A. Levina, P. A. Lay, *J. Am. Chem. Soc.* **2019**, submitted.
- [50] E. Bioscience, IncuCute Caspase-3/7 reagent for Apoptosis, **2018**.
- [51] E. Bioscience, IncuCute Cytotox red reagent for counting dead cells, **2018**.
- [52] A. Levina, J. B. Aitken, Y. Y. Gwee, Z. J. Lim, M. Liu, A. M. Singharay, P. F. Wong, P. A. Lay, *Chem. - Eur. J.* **2013**, *19*, 3609-3619.
- [53] A. Saraste, K. Pulkki, *Cardiovasc. Res.* **2000**, *45*, 528-537.
- [54] a) U. Ziegler, P. Groscurth, *News Physiol Sci* **2004**, *19*, 124-128; b) R. Andrade, L. Crisol, R. Prado, M. D. Boyano, J. Arluzea, J. Arechaga, *Biol. Cell* **2010**, *102*, 25-35.

FULL PAPER

- [55] F. Lentz, A. Drescher, A. Lindauer, M. Henke, R. A. Hilger, C. G. Hartinger, M. E. Scheulen, C. Dittrich, B. K. Keppler, U. Jaehde, *Anti-Cancer Drugs* **2009**, *20*, 97-103.
- [56] a) M. D. Hall, M. Okabe, D.-W. Shen, X.-J. Liang, M. M. Gottesman, *Annu. Rev. Pharmacol. Toxicol.* **2008**, *48*, 495-535; b) B. Zhitomirsky, Y. G. Assaraf, *Oncotarget* **2017**, *8*, 45117-45132.
- [57] W.-M. Li, L.-L. Zhou, M. Zheng, J. Fang, *Mol. Ther.--Nucleic Acids* **2018**, *12*, 707-717.
- [58] J. Pracharova, V. Novohradsky, H. Kostrhunova, P. Starha, Z. Travnicek, J. Kasparkova, V. Brabec, *Dalton Trans.* **2018**, *47*, 12197-12208.
- [59] H. V. R. Silva, J. S. M. Dias, G. A. Ferreira-Silva, L. C. Vegas, M. Ionta, C. C. Correa, A. A. Batista, M. I. F. Barbosa, A. C. Doriguetto, *Polyhedron* **2018**, *144*, 55-65.
- [60] C. P. Popolin, J. P. B. Reis, A. B. Becceneri, A. E. Graminha, M. A. P. Almeida, R. S. Correa, L. A. Colina-Vegas, J. Ellena, A. A. Batista, M. R. Cominetti, *PLoS One* **2017**, *12*, e0183275/0183271-e0183275/0183221.
- [61] a) W. Cao, W. Zheng, T. Chen, *Sci. Rep.* **2015**, *5*, 9157; b) A. Tadic, J. Poljarevic, M. Krstic, M. Kajzerberger, S. Arandjelovic, S. Radulovic, C. Kakoulidou, A. N. Papadopoulos, G. Psomas, S. Grguric-Sipka, *New J. Chem.* **2018**, *42*, 3001-3019.
- [62] K. Togami, K. Yamaguchi, S. Chono, H. Tada, *J. Pharmacol. Toxicol. Methods* **2017**, *86*, 19-27.
- [63] J. Swanner, J. Mims, D. L. Carroll, S. A. Akman, C. M. Furdui, S. V. Torti, R. N. Singh, *Int. J. Nanomed.* **2015**, *10*, 3937-3953.
- [64] a) E. Schreiber-Brynzak, E. Klapproth, C. Unger, I. Lichtscheidl-Schultz, S. Goeschl, S. Schweighofer, R. Trondl, H. Dolznig, M. A. Jakupec, B. K. Keppler, *Invest. New Drugs* **2015**, *33*, 835-847; b) G. K. Gransbury, P. Kappen, C. J. Glover, J. N. Hughes, A. Levina, P. A. Lay, I. F. Musgrave, H. H. Harris, *Metalomics* **2016**, *8*, 762-773.
- [65] P. A. Marks, R. Breslow, *Nat. Biotechnol.* **2007**, *25*, 84-90.
- [66] M. Senko, Sunnyvale, CA, USA, **1998**.
- [67] a) R. I. Freshney, *Culture of Animal Cells: A Manual of Basic Technique and Specialized Applications, 7th Edition.*, Wiley-Blackwell, Hoboken, NJ, USA, **2016**; b) A. Levina, H. H. Harris, P. A. Lay, *J. Am. Chem. Soc.* **2007**, *129*, 1065-1075.
- [68] M. S. Inc., Northampton, MA, USA, **1999**.
- [69] A. Levina, T. H. N. Pham, P. A. Lay, *Angew. Chem., Int. Ed.* **2016**, *55*, 8104-8107.
- [70] M. P. Jensen, D. Gorman-Lewis, B. Aryal, T. Paunesku, S. Vogt, P. G. Rickert, S. Seifert, B. Lai, G. E. Woloschak, L. Soderholm, *Nat. Chem. Biol.* **2011**, *7*, 560-565.

Table 2. Cell lines used for testing the anti-proliferative activities of Ru(II)-arene-thiocarboxylato dimers.

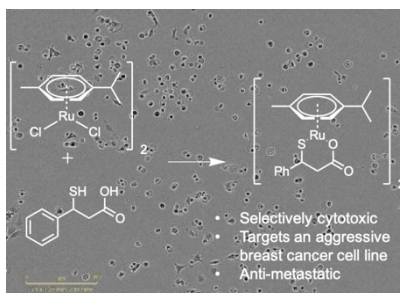
No. ^a	Cell line	ATCC ^b No.	Species	Tissue	Disease	Phenotype
1	THP-1	TIB-202	human	peripheral blood	acute monocytic leukemia	non-adherent
2	HL-60	CCL-240	human	peripheral blood	acute promyelocytic leukemia	non-adherent
3	MDA-MB-231	HTB-26	human	mammary gland ^f	adenocarcinoma	mesenchymal ^g
4	HT-1080	CCL-121	human	connective tissue	fibrosarcoma	mesenchymal ^g
5	A2780cis ^c	93112517 ^e	human	ovaries	adenocarcinoma	mixed ^h
6	A2780 ^d	93112519 ^e	human	ovaries	adenocarcinoma	epithelial
7	HEK-293	CRL-1573	human	embryonic kidney	normal (virus-immortalized)	epithelial
8	PC-3	CRL-1435	human	prostate	adenocarcinoma	epithelial
9	MCF-7	HTB-22	human	mammary gland ^f	adenocarcinoma	epithelial
10	BEAS-2B	CRL-9609	human	lung, bronchus	normal (virus-immortalized)	epithelial
11	A549	CCL-185	human	lung	carcinoma	epithelial
12	PANC-1	CRL-1469	human	pancreas/duct	epithelioid carcinoma	epithelial
13	HepG2	HB-8065	human	liver	hepatocellular carcinoma	epithelial
14	V79-4	CCL-93	hamster	lung	normal	fibroblasts
15	3T3-L1	CL-173	mouse	embryo	normal	fibroblasts

^a Numbering corresponds to that in Figure 7. ^b American Type Culture Collection (ATCC). ^c Cisplatin-resistant clone, IC_{50} for cisplatin $5.4 \pm 0.5 \mu\text{M}$ (72 h treatment, MTT assay).⁵⁹ ^d Cisplatin-sensitive clone, IC_{50} for cisplatin $0.93 \pm 0.05 \mu\text{M}$ (72 h treatment, MTT assay).⁵⁹ ^e European Collection of Authenticated Cell Cultures (ECACC). ^f Derived from lung metastases. ^g Although classified as epithelial by ATCC, these cell lines exhibit mesenchymal-like properties, including elongated morphology, low expression of E-cadherin and high expression of vimentin, formation of protrusions, and invasion through extracellular matrix in the absence of added growth factors.^{35, 55} ^h Cisplatin resistance in A2780 cells is acquired by partial conversion from epithelial to mesenchymal phenotype.

FULL PAPER

FULL PAPER

A sulfidocarboxylato Ru(II) (*p*-cymene) complex; [Ru(*p*-cymene)(MPP)]₂, derived from 3-mercapto-3-phenylpropanoic acid (MPP), demonstrates strong ligand dependency in displaying selective anti-metastatic activity towards a highly aggressive breast cancer cell line.



L. J. Stephens, A. Levina, I. Trinh, V. L. Blair, M. V. Werrett, P. A. Lay and P. C. Andrews**

Page No. – Page No.

A Stable Ruthenium(II)-Arene Thiocarboxylato Dimer is Selectively Cytotoxic to Invasive Breast Cancer Cells